A Fully Soft-Switched Single Switch Isolated DC–DC Converter

Minjae Kim, *Student Member, IEEE*, and Sewan Choi, *Senior Member, IEEE*

***Abstract*—This paper proposes a soft-switched single switch isolated converter. The proposed converter is able to offer low cost and high power density in step-up application due to the following features: zero-current switching (ZCS) turn-on and zero-voltage switching (ZVS) turn-off of switch and ZCS turn-off of diodes regardless of voltage and load variation; low rated lossless snubber; reduced transformer volume compared to flyback-based converters due to low magnetizing current. Experimental results on a 100 kHz, 250 W prototype are provided to validate the proposed concept.**

***Index Terms*—Isolated step-up dc–dc converter, single switch, soft switching.**

I. Introduction

ISOLATED step-up dc–dc converters are used in many applications, such as photovoltaic module-integrated converter (MIC) systems, portable fuel cell systems, and vehicle inverters where high efficiency, high power density, and low cost are required [1]–[4]. Owing to smaller input current ripple, lower diode voltage rating and lower transformer turns ratio, the current-fed isolated converter is better suited for step-up applications. The current-fed isolated converter has two types: passive-clamped [5]–[7] and active-clamped [8]–[13]. The passive-clamped current-fed converter has simple structure and small switch count, but suffers from excessive power losses dissipated in the RCD snubber and associated with hard switching of main switch. Active-clamped current-fed converters have actively been developed based on three basic topologies: push–pull [8], full-bridge [9], [10], and half-bridge [11]–[13]. They achieve not only lossless clamping of voltage spikes caused by transformer leakage inductance but also zero-voltage switching (ZVS) turn on of switches. However, they may not be expected to achieve high efficiency and low cost in relatively low power application since they need at least four switches and gate driver circuits.

Isolated converters with reduced switch count have been proposed for low power application [14]–[26]. Isolated dc–dc converters with one main switch and one clamp switch achieve ZVS turn on of switches, but switches are turned off with hard switching [14]–[17]. Isolated single switch dc–dc converters are more attractive to achieve low cost [18]–[26]. *Z*-source converter [18], [19] and flyback converter [20]–[23] are hard switched at both turn-on and turn-off instants. Frequency-controlled flyback converter [24] and series-connected forward-flyback converter [25] achieve zero-current switching (ZCS) turn-on of switch, but the switch is hard switched at turn-off instant. The aforementioned single switch topologies have increased transformer volume since magnetizing inductor is used for energy transfer. An isolated single-switch resonant converter [26] achieves both ZCS turn-on and ZCS turn-off of switch, but need high transformer turn ratio for step-up application due to low voltage gain and hence is not suited to step-up application.

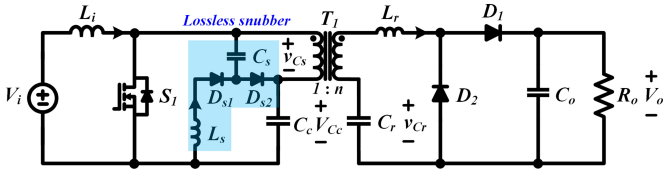

Fig. 1. Proposed isolated single switch ZCS–ZVS converter.

In this paper, a soft-switched single switch isolated converter is proposed for step-up application. The proposed converter has the following features: 1) ZCS turn-on and ZVS turn-off of switch regardless of voltage and load variation; 2) ZCS turn-off of all diodes leading to negligible voltage surge associated with the diode reverse recovery; 3) small input current ripple due to CCM operation; 4) reduced transformer volume due to low magnetizing current; and 5) low-rated lossless snubber, which makes it possible to achieve high efficiency and low cost for step-up application. Experimental results on a 100 kHz, 250 W prototype are provided to validate the proposed concept.

II. Proposed Converter

Fig. 1 shows the circuit diagram of the proposed converter. The proposed converter consists of input filter inductor L_i, switch S_1, a lossless snubber which includes capacitor C_s, inductor L_s, and diodes D_{s1} and D_{s2}, and clamp capacitor C_c at the primary side and L_r–C_r series resonant circuit and diodes D_1 and D_2 at the secondary side. The lossless snubber makes it possible to achieve ZVS turn-off of switch as well as clamp the voltage spikes of the switch by leakage inductance. Also, the $L_{\rm r}$–$C_{\rm r}$ series resonant circuit makes it possible to achieve ZCS turn-off of diodes. Fig. 2 shows three resonance operations according to the variations of resonant frequency f_{r1} which is expressed as in (1): the above-resonance operation ($DT_s < 0.5T_{r1}$), the resonance operation ($DT_s = 0.5T_{r1}$), and

Manuscript received July 1, 2014; revised August 29, 2014; accepted October 7, 2014. Date of publication October 20, 2014; date of current version April 15, 2015. This work was supported by the National Research Foundation of Korea (NRF) grant funded by the Korea government (MSIP) (No. 2014R1A2A2A01003724). Recommended for publication by Associate Editor T.-J. Liang.

M. Kim is with the Department of New Energy Engineering, Seoul National University of Science and Technology, Seoul 139-743, Korea (e-mail: tostood@seoultech.ac.kr).

S. Choi is with the Department of Electrical & Information Engineering, Seoul National University of Science and Technology, Seoul 139-743, Korea (e-mail: schoi@seoultech.ac.kr).

Color versions of one or more of the figures in this paper are available online at http://ieeexplore.ieee.org.

Digital Object Identifier 10.1109/TPEL.2014.2363830

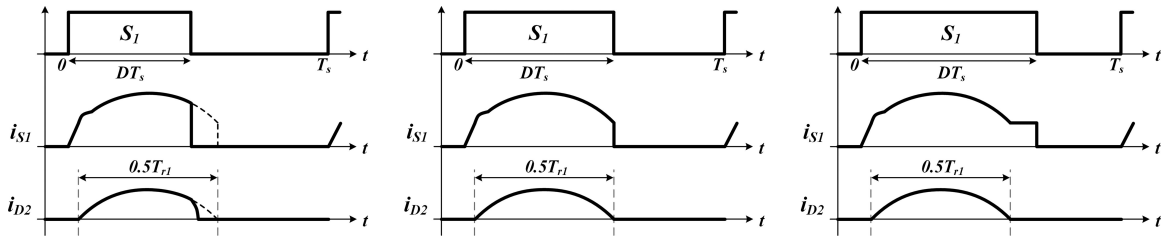

Fig. 2. Comparison of switch and diode current waveform according to variation of f_{r1}: (a) above-resonance operation ($DT_s < 0.5T_{r1}$), (b) resonance operation ($DT_s = 0.5T_{r1}$), and (c) below-resonance operation ($DT_s > 0.5T_{r1}$).

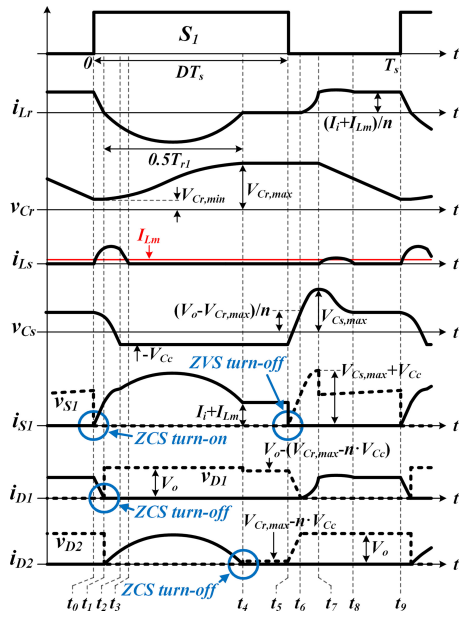

Fig. 3. Key waveforms of the proposed converter in the below-resonance operation.

the below-resonance operation ($DT_s > 0.5T_{r1}$)

$$f_{r1} = \frac{1}{T_{r1}} = \frac{1}{2\pi\sqrt{L_r C_r}}. \tag{1}$$

It can be seen from Fig. 2 that the total switching losses are smaller for the below-resonance operation since both switch turn-off current and diode *di/dt* of the below-resonance operation are smaller than them of the above-resonance operation. Therefore, the below-resonance operation is chosen for the proposed converter.

A. Operating Principles

Figs. 3 and 4 show key waveforms and operation states of the proposed converter in the below-resonance operation, respectively. In order to simplify the analysis of the steady-state operation, it is assumed that the input filter and magnetizing inductances are large enough so that they can be treated as constant current sources during a switching period. It is also assumed that clamp and output capacitances are large enough so that they can be treated as constant voltage sources during a switching period. The voltage V_{Cc} across the clamp capacitor is the same as the input voltage V_i. In the below-resonance operation, nine modes exist within T_s.

Mode 1 (t_0–t_1): This mode begins when switch S_1 is turned ON. Equivalent circuit of this mode is shown in Fig. 5(a). L_s and C_s start resonating and resonant current i_{Ls} flows through L_s, D_{s1}, C_s, and S_1. The voltage and current of resonant components are determined, respectively, as follows:

$$i_{Ls}(t) = v_{Cs}(t_0)\sqrt{\frac{C_s}{L_s}}\sin(\omega_{r2}(t-t_0)), \quad t_0 < t < t_2 \tag{2}$$

$$v_{Cs}(t) = v_{Cs}(t_0)\cos(\omega_{r2}(t-t_0)), \quad t_0 < t < t_2 \tag{3}$$

where $\omega_{r2} = 1/\sqrt{L_s C_s}$. Since induced voltage $V_{Cr,\min}$–nV_{Cc}–V_o across L_r makes time interval from t_0 to t_1 very short, current i_{Lr} appears to decrease almost linearly. Current through S_1 increases with the slope of i_{Lr}, resulting in ZCS turn-on of S_1. The turn-on loss of switch associated with energy stored in MOSFET's output capacitance is negligible in this low input voltage application [27]–[29]. This mode ends when current i_{Lr} reaches 0 A. It is noted that diode D_1 is turned OFF under ZCS condition.

Mode 2 (t_1–t_2): This mode begins when current i_{Lr} changes its direction. Equivalent circuit of this mode is shown in Fig. 5(b). L_r and C_r start resonating and resonant current i_{Lr} flows through L_r, C_r, and D_2. The voltage and current of resonant components are determined, respectively, as follows:

$$i_{Lr}(t) = (V_{Cr,\min} - nV_{Cc})\sqrt{\frac{C_r}{L_r}}\sin(\omega_{r1}(t-t_1)), \quad t_1 < t < t_4 \tag{4}$$

$$v_{Cr}(t) = nV_{Cc} - (nV_{Cc} - V_{Cr,\min})\cos(\omega_{r1}(t-t_1)), \quad t_1 < t < t_4 \tag{5}$$

where $\omega_{r1} = 1/\sqrt{L_r C_r}$. When voltage across snubber capacitor C_s equals $-V_{Cc}$, L_s–C_s resonance ends.

Mode 3 (t_2–t_3): This mode begins when diode D_{s2} is turned ON. Current i_{Ls} is determined by following equation, and this mode ends when current i_{Ls} reaches 0 A

$$i_{Ls}(t) = -\frac{V_{Cc}}{L_s}(t-t_2) + i_{Ls}(t_2), \quad t_2 < t < t_3. \tag{6}$$

It is noted that diodes D_{s1} and D_{s2} are turned OFF under ZCS condition.

Mode 4 (t_3–t_4): The L_r–C_r resonance keeps on during this mode and ends when current i_{Lr} reaches 0 A. Note that diode D_2 is turned OFF under ZCS condition.

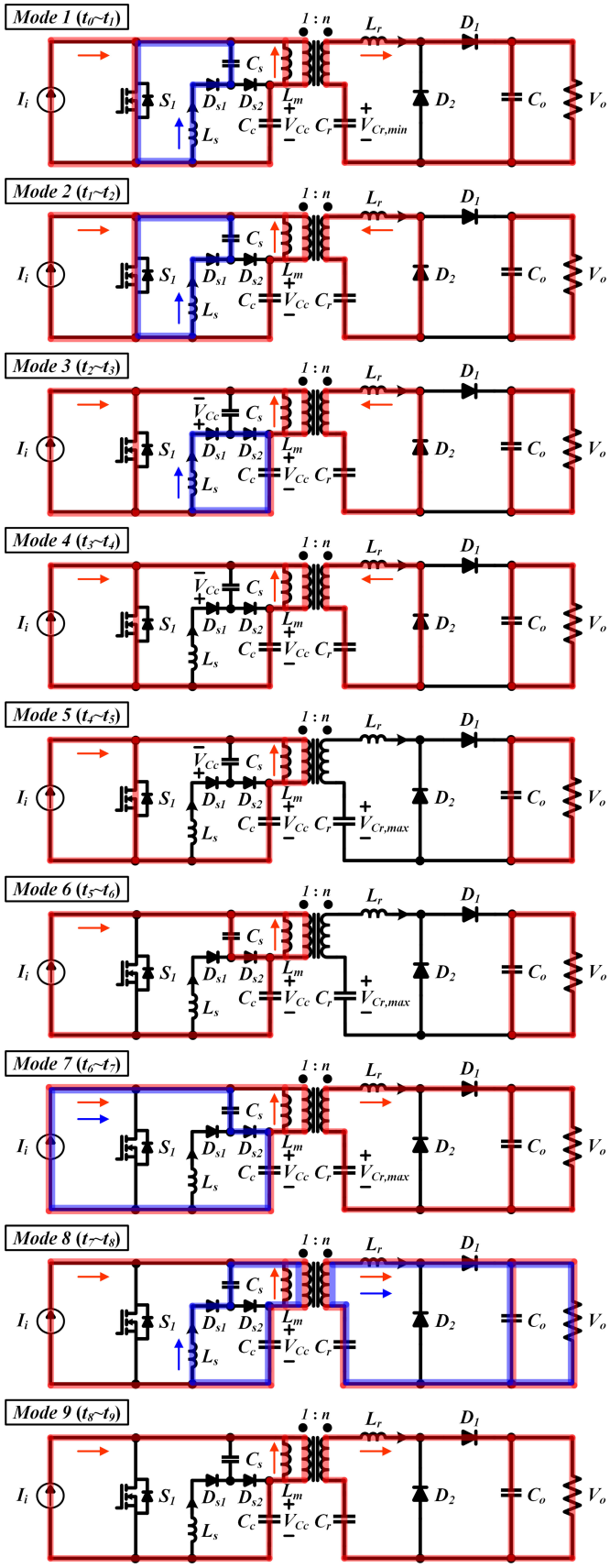

Fig. 4. Operation states of the proposed converter in the below-resonance operation.

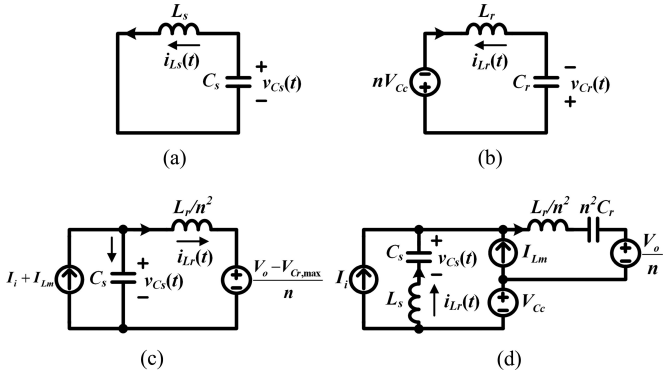

Fig. 5. Equivalent resonant circuits. (a) Mode 1–2 (t_0–t_2). (b) Mode 2–4 (t_1–t_4). (c) Mode 7 (t_6–t_7). (d) Mode 8 (t_7–t_8).

Mode 5 (t_4–t_5): During this mode, a constant current flows through S_1 whose value is the sum of the input current I_i and the magnetizing current I_{Lm}.

Mode 6 (t_5–t_6): The mode begins when S_1 is turned OFF. Then, $I_i + I_{Lm}$ flows through C_s, D_{s2}, and C_c. Voltage across snubber capacitor C_s which is determined by the following equation increases linearly with the slope of $(I_i + I_{Lm})/C_s$, resulting in ZVS turn-off of S_1

$$v_{Cs}(t) = \frac{I_i + I_{Lm}}{C_s}(t - t_5) - V_{Cc}, \quad t_5 < t < t_6. \tag{7}$$

This mode ends when v_{Cs} becomes equal to $(V_o - V_{Cr,\max})/n$.

Mode 7 (t_6–t_7): This mode begins when diode D_1 is turned ON. Equivalent circuit of this mode is shown in Fig. 5(c). L_r and C_s start resonating and resonant current i_{Lr} flows through C_s, D_{s2}, L_r, $D_{1,}$ and C_r. Assuming that $C_s << n^2 C_r$, v_{Cr} can be considered constant, and resonance frequency ω_{r3} can be determined by C_s and L_r. Therefore, the voltage and current of resonant components are determined, respectively, as follows:

$$i_{Lr}(t) = (I_i + I_{Lm})[1 - \cos(\omega_{r3}(t - t_6))], \quad t_6 < t < t_7 \tag{8}$$

$$v_{Cs}(t) = \frac{I_i + I_{Lm}}{n}\sqrt{\frac{L_r}{C_s}}\sin(\omega_{r3}(t - t_6)) + \frac{V_o - V_{Cr,\max}}{n}, \quad t_6 < t < t_7 \tag{9}$$

where $\omega_{r3} = n/\sqrt{L_r C_s}$. This mode ends when current i_{Lr} becomes equal to $(I_i + I_{Lm})/n$.

Mode 8 (t_7–t_8): This mode begins when diode D_{s1} is turned ON. Equivalent circuit of this mode is shown in Fig. 5(d). L_s, C_s, L_r, and C_r start resonating and resonant current i_{Lr} flows through $L_s, D_{s1}, C_s, C_c, L_r, D_1$, and C_r. Assuming that $C_s << n^2 C_r$ and $L_s \gg L_r/n^2$, the voltage and current of resonant components are determined using the superposition principle, respectively, as follows:

$$i_{Ls}(t) = \left[V_{Cc} + \frac{V_o}{n} - \left(V_{Cs,\max} + \frac{V_{Cr,\max}}{n}\right)\right] \times \sqrt{\frac{C_s}{L_s}}\sin(\omega_{r2}(t - t_7)), \quad t_7 < t < t_8 \tag{10}$$

$$v_{Cs}(t) = \left[V_{Cc} + \frac{V_o}{n} - \left(V_{Cs,\max} + \frac{V_{Cr,\max}}{n}\right)\right] \times [1 - \cos(\omega_{r2}(t - t_7))] + V_{Cs,\max}, \quad t_7 < t < t_8. \tag{11}$$

Assuming that $i_{Lr} \approx (I_i + I_{Lm})/n$ during this mode, voltage v_{Cr} is determined by the following equation:

$$v_{Cr}(t) = -\frac{I_i + I_{Lm}}{nC_r}(t - t_7) - V_{Cr,\max}, \quad t_7 < t < t_9. \tag{12}$$

This mode ends when current i_{Ls} reaches 0 A.

Mode 9 (t_8–t_9): Switch S_1 is in the turn-off state, and the sum of the input current and magnetizing current is being transferred to the secondary. Current i_{D1} is equal to $(I_i + I_{Lm})/n$. This mode ends when switch S_1 is turned ON.

The average current of magnetizing inductor L_m is equal to average current of snubber inductor L_s since $I_{Ls,\text{avg}} = I_{Ds2,\text{avg}}$ and $I_{Ds2,\text{avg}} = I_{Lm,\text{avg}}$. Therefore, it should be noted that transformer core volume of the proposed converter is much smaller compared to that of the flyback-based converter since $I_{Ls,\text{avg}} (= I_{Lm,\text{avg}})$ can be designed to be small.

B. Voltage Gain Expression

To obtain voltage gain of the proposed converter, it is assumed that voltage across C_c is constant and magnetizing current is ignored during the switching period T_s.

1) Below-Resonance Operation ($DT_s > 0.5T_{r1}$): Since the average current of diode D_2 is identical to the average load current in the steady state, the following equation is obtained:

$$I_{D2,\text{avg}} = \frac{V_o}{R_o} = \frac{1}{T_s}\int_{t_1}^{t_4} i_{D2}(t)dt = \frac{1}{T_s}\int_{t_1}^{t_4} -i_{Lr}(t)dt. \tag{13}$$

From (4) and (13), minimum voltage of the resonant capacitor $V_{Cr,\min}$ can be obtained by

$$V_{Cr,\min} = nV_{Cc} - \frac{V_o}{2C_r f_s R_o}. \tag{14}$$

From (5) and (14), maximum voltage of the resonant capacitor $V_{Cr,\max}$ can be obtained by

$$V_{Cr,\max} = nV_{Cc} + \frac{V_o}{2C_r f_s R_o}. \tag{15}$$

The time interval from t_7 to t_9 in Fig. 3 can be obtained from (12) and (15) by

$$t_9 - t_7 = \frac{nV_o}{I_i f_s R_o}. \tag{16}$$

The time interval from t_5 to t_6 in Fig. 3 can be obtained from (7) by

$$t_6 - t_5 = \frac{C_s}{I_i}\left(\frac{V_o - V_{Cr,\max}}{n} + V_{Cc}\right). \tag{17}$$

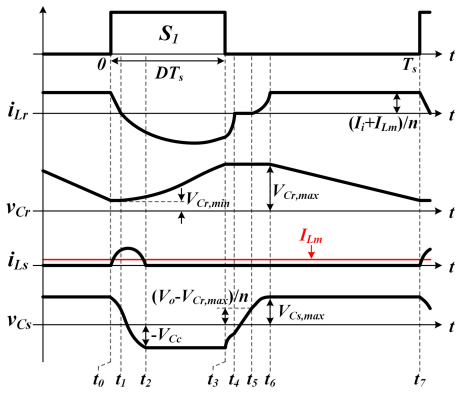

Fig. 6. Key waveforms of the proposed converter in the above-resonance operation.

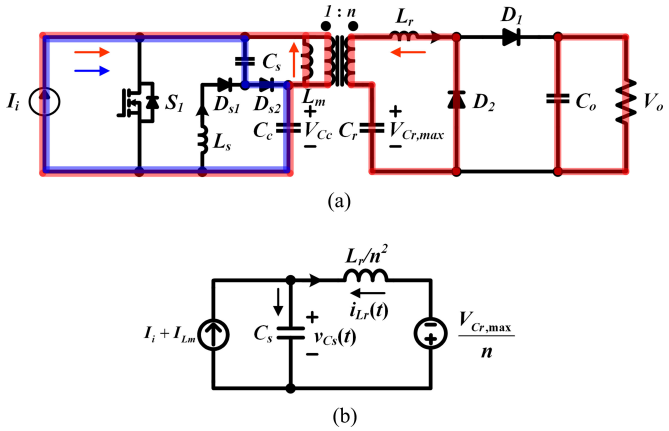

Fig. 7. Operation at time interval from t_3 to t_4 in above resonance: (a) operation state. (b) Equivalent resonant circuit.

The time interval from t_6 to t_7 in Fig. 3 is quarter the L_r–C_s resonant frequency and determined by

$$t_7 - t_6 = \frac{\pi}{2\omega_{r3}}. \tag{18}$$

By applying (16)–(18) to $(1\text{–}D)T_s$, the voltage gain can be obtained by

$$\frac{V_o}{V_i} = \frac{n + B}{1 - D - A} \tag{19}$$

where $A = \frac{\pi f_s}{2\omega_{r3}}$ and $B = \frac{C_s(2C_r f_s R_o - 1)}{2nC_r}$.

2) Above-Resonance Operation ($DT_s < 0.5T_{r1}$): Fig. 6 shows key waveforms of the proposed converter in the above-resonance operation. The operating principles of the above resonance are the same as that of the below resonance except time interval from t_3 to t_4. Assuming that $C_s << n^2 C_r$, an equivalent circuit of time interval from t_3 to t_4 is shown in Fig. 7(b). The time interval from t_0 to t_3 can be approximated as DT_s. Since the average current of diode D_2 is identical to the average load current, it can be approximated by

$$I_{D2,\text{avg}} = \frac{V_o}{R_o} \approx \frac{1}{T_s}\int_0^{DT_s} i_{D2}(t)dt \approx \frac{1}{T_s}\int_0^{DT_s} -i_{Lr}(t)dt. \tag{20}$$

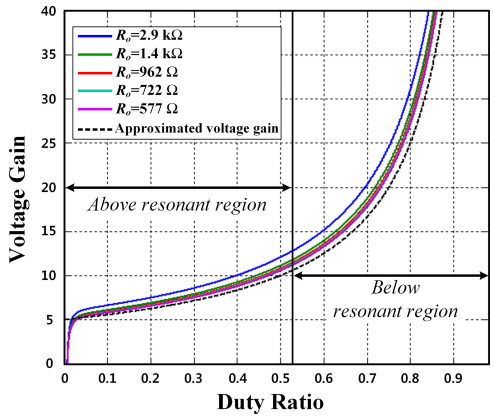

Fig. 8. Voltage gain of the proposed converter ($V_i = 28$ V, $L_r = 5$ μH, $C_r = 560$ nF, $L_s = 5$ μH, $C_s = 16$ nF, $n = 5$, $f_s = 100$ kHz).

From (4) and (20), minimum voltage of the resonant capacitor $V_{Cr,\min}$ can be obtained by

$$V_{Cr,\min} = nV_{Cc} - \frac{V_o}{C_r f_s R_o (1 - \cos(\omega_{r1} DT_s))}. \quad (21)$$

From (5) and (21), maximum voltage of the resonant capacitor $V_{Cr,\max}$ can be obtained by

$$V_{Cr,\max} = nV_{Cc} - \frac{V_o \cos(\omega_{r1} DT_s)}{C_r f_s R_o (1 - \cos(\omega_{r1} DT_s))}. \quad (22)$$

The time interval from t_6 to t_7 in Fig. 6 can be obtained from (12) and (22) by

$$t_7 - t_6 = \frac{nV_o}{I_i f_s R_o}. \quad (23)$$

Assuming that $dv_{Cs}/dt \approx I_i/C_s$ during the time interval from t_3 to t_5 in Fig. 6, this time interval can be obtained from (7) by

$$t_5 - t_3 = \frac{C_s}{I_i}\left(\frac{V_o - V_{Cr,\max}}{n} + V_{Cc}\right). \quad (24)$$

The time interval from t_5 to t_6 in Fig. 6 is quarter the L_r–C_s resonant frequency and determined by

$$t_6 - t_5 = \frac{\pi}{2\omega_{r3}}. \quad (25)$$

By applying (23)–(25) to (1–*D*)T_s, the voltage gain can be obtained by

$$\frac{V_o}{V_i} = \frac{n + C}{1 - D - A} \quad (26)$$

where $C = \frac{C_s[C_r f_s R_o (1-\cos(\omega_{r1} DT_s)) - \cos(\omega_{r1} DT_s)]}{nC_r(1-\cos(\omega_{r1} DT_s))}$.

Using (19) and (26), the voltage gain of the proposed converter is plotted as shown in Fig. 8.

C. Design Procedure

In this section, a design procedure of the proposed converter is presented with an example. A specification for the design example is given as follows: output power $P_o = 250$ W, output voltage $V_o = 380$, input voltage $V_i = 28$–38 V, and switching frequency $f_s = 100$ kHz.

1) Choose Average Value of Snubber Inductor Current $I_{Ls,\text{avg}}$: $I_{Ls,\text{avg}}$ should be as small as possible in order to minimize conduction loss of the snubber components and magnitude of the magnetizing current. It is seen from (2) and (10) that $I_{Ls,\text{avg}}$ is proportional to the snubber capacitance C_s. However, if C_s is chosen to be small to reduce conduction loss of the snubber components, the voltage rating of the switch increases, as shown in (9), resulting in high conduction loss of the switch. Therefore, considering tradeoff between conduction losses of the switch and snubber components, $I_{Ls,\text{avg}}$ is chosen to be around 3% of average input current, which is expressed as

$$I_{Ls,\text{avg}} = 0.03 I_{i,\text{avg}} = 0.27\,\text{A}. \quad (27)$$

2) Determine Values of n, L_r, and C_r: In order to simplify the design procedure, the voltage gain can be approximated as

$$\frac{V_o}{V_i} \approx \frac{n}{1 - D}. \quad (28)$$

As mentioned earlier, the below-resonance operation is chosen for the proposed converter due to smaller switch turn-off current and diode *di/dt*. From Fig. 2, the minimum duty cycle for the below-resonance operation can be obtained by

$$D_{\min} = \pi f_s \sqrt{L_r C_r}. \quad (29)$$

Since resonant inductance L_r should be designed to minimize reverse-recovery effects of diode D_1, the time interval from t_0 to t_1 in Fig. 3 should be greater than $3t_{rr1}$, which is expressed as

$$t_1 - t_0 = 3t_{rr1} = \frac{(I_i + I_{Lm})L_r}{nV_o(1 + 1/2C_r f_s R_o)} \quad (30)$$

where t_{rr1} is reverse-recovery time of diode D_1.

Based on the operating principles, the RMS current and turn-on voltage of switch S_1 can be obtained, respectively, as follows:

$$I_{S1,\text{rms}} \approx \sqrt{D} I_i + \frac{n\pi I_o}{2\sqrt{2D_{\min}}}, \quad (D_{\min} < D < D_{\max}) \quad (31)$$

$$V_{S1,\text{on}} = v_{S1}(t_0) = \frac{V_o - V_{Cr,\min}}{n} + V_{Cc}. \quad (32)$$

Fig. 9 shows RMS current and turn-on voltage of switch S_1 based on (28)–(32) with different values of *n*. In this example, the turn ratio of the transformer *n* is chosen to be 5 considering tradeoff of conduction loss and switching loss of switch S_1. Resonant values L_r and C_r are determined by 5 μH and 560 nF, respectively, using (28)–(30).

3) Determine Value of C_s: $I_{Ls,\text{avg}}$ can be obtained by, using (2), (6), and (10)

$$I_{Ls,\text{avg}} = \frac{C_s}{T_s}\left[v_{Cs}(t_0) + 3V_{Cc} - 2V_{Cs,\max} + \frac{2(V_o - V_{Cr,\max})}{n} + 0.5 v_{Cs}(t_0) \sin\left(\cos^{-1}\left(\frac{-V_{Cc}}{v_{Cs}(t_0)}\right)\right) \cos^{-1}\left(\frac{-V_{Cc}}{v_{Cs}(t_0)}\right)\right] \quad (33)$$

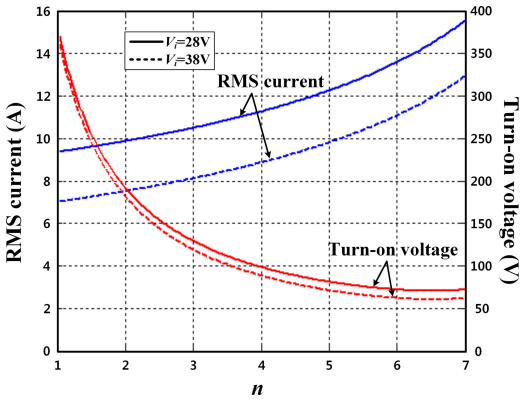

Fig. 9. RMS current and turn-on voltage of switch S_1 with different values of n.

where $v_{Cs}(t_0) = 2(V_{Cc} + \frac{V_o - V_{Cr,\max}}{n}) - V_{Cs,\max}$ and $V_{Cs,\max} = \frac{I_i + I_{Lm}}{n}\sqrt{\frac{L_r}{C_s}} + \frac{V_o - V_{Cr,\max}}{n}$.

By applying n, L_r, C_r, and (27) to (33), snubber capacitance C_s can be calculated as 16 nF.

4) Determine Value of L_s: Snubber inductance L_s should be designed to minimize reverse-recovery effects of snubber diodes D_{s1} and D_{s2}. Therefore, the time interval from t_2 to t_3 in Fig. 3 should be greater than $3t_{rr2}$, which is expressed as

$$t_3 - t_2 = 3t_{rr2} = \frac{v_{Cs}(t_0) L_s \sin(\cos^{-1}(-V_i/v_{Cs}(t_0)))}{V_i}\sqrt{\frac{C_s}{L_s}} \quad (34)$$

where t_{rr2} is reverse-recovery time of diodes D_{s1} and D_{s2}.

According to (34), snubber inductance L_s is calculated as 5 μH.

5) Select Semiconductor Devices: Semiconductor devices of the proposed converter are selected based on the previous design procedure and operating principles. It can be seen from Fig. 3 that output diodes D_1 and D_2 have a maximum voltage stress of V_o. Peak current of output diode D_2 is $0.5\pi I_o/D_{\min}$ from (13). Maximum voltage stress across the switch S_1 is determined by

$$V_{S1,\max}(t) = \frac{I_i + I_{Lm}}{n}\sqrt{\frac{L_r}{C_s}} + \frac{V_o - V_{Cr,\max}}{n} + V_{Cc}. \quad (35)$$

Current stress of switch S_1 is determined by (31). As shown in Figs. 3 and 4, maximum voltage stresses across snubber diodes D_{s1} and D_{s2} are $v_{Cs}(t_0) + V_{Cc}$ and V_{Cc}, respectively. Peak currents of snubber diodes D_{s1} and D_{s2} are $v_{Cs}(t_0)\sqrt{C_s/L_s}$ from (2) and I_i, respectively. Selected devices and component ratings according to the previous design procedure are shown in Table I.

TABLE I
COMPONENT RATINGS AND SELECTED DEVICES

Components		Rating	Selected devices
Switch S_1	$V_{\rm pk}$	110 V	IRFP4568
	$I_{\rm rms}$	11.8 A	
Snubber diodes D_{s1}, D_{s2}	$V_{\rm pk}$	94 V	UG8DT
	$I_{\rm avg}$	0.27 A	
Output diodes D_1, D_2	$V_{\rm pk}$	380 V	VS-HFA04TB60
	$I_{\rm avg}$	0.65 A	
Filter inductor L_i	Inductance	100 μH	Ferrite core PQ32/30
	$I_{\rm rms}$	8.85 A	
Snubber inductor L_s	Inductance	5 μH	Ferrite core EF16
	$I_{\rm rms}$	0.8 A	
Snubber capacitor C_s	Capacitance	16 nF	BFC241941603
	$V_{\rm pk}$	82 V	
	$I_{\rm rms}$	1.4 A	
Clamp capacitor C_c	Capacitance	82 μF	FFB44D0826K
	$V_{\rm pk}$	38 V	
	$I_{\rm rms}$	7.6 A	
Transformer T_1	Leakage inductance	5 μH	Ferrite core PQ32/30
	Magnetizing inductance	93 μH	
	Turn ratio	1:5	
	VA	273VA	
Resonant capacitor C_r	Capacitance	560 nF	ECW-FD2W564K4
	$V_{\rm pk}$	196 V	
	$I_{\rm rms}$	1.6 A	
Output capacitor C_o	Capacitance	1 μF	ECQ-E2W105KH
	$V_{\rm pk}$	380 V	
	$I_{\rm rms}$	0.87 A	

III. EXPERIMENTAL RESULT

A 250 W laboratory prototype of the proposed converter has been built and tested to verify the proposed concept. Component ratings and selected devices of the proposed converter are listed in Table I. We can see from Table I that current ratings of the snubber components are much lower than those of main components. Leakage inductance of the transformer is used as the resonant inductance. Figs. 10 and 11 show experimental waveforms at full-load and half-load conditions when input voltage is 28 V, respectively. Figs. 10(a) and 11(a) show that switch S_1 is turned ON with ZCS at both full- and half-load conditions. Figs. 10(b) and 11(b) show the experimental waveforms of switch S_1 at turn-off. In theory, S_1 is turned OFF with ZVS. However, it is seen from Figs. 10(b) and 11(b) that S_1 generate small amount of losses due to ringing caused by parasitic resonance between MOSFET's output capacitance and parasitic inductances in prototype circuit. This loss could be reduced with professional manufacturing techniques.

Figs. 10(c) and 11(c) show that diode D_1 is turned OFF with ZCS at both conditions. Figs. 10(d) and 11(d) show that diode D_2 is turned OFF with ZCS at both conditions. Figs. 10(e) and 11(e) show waveforms of i_{Lr} and v_{Cr}, which are in close agreement with the analytical waveforms shown in Fig. 3. Voltages $V_{Cr,\max}$ at both conditions are measured to be 143.1 and 142.5 V, respectively. They are close to analytical values of 145.8 and 143 V obtained from (14) and (15). Figs. 10(f) and 11(f) show waveform of v_{Cs}.

Fig. 12 shows the theoretical and experimental voltage gains of the proposed converter under $V_i = 28$ V, $R_o = 577\ \Omega$. The experimental voltage gain is in close agreement with the theoretical voltage gain.

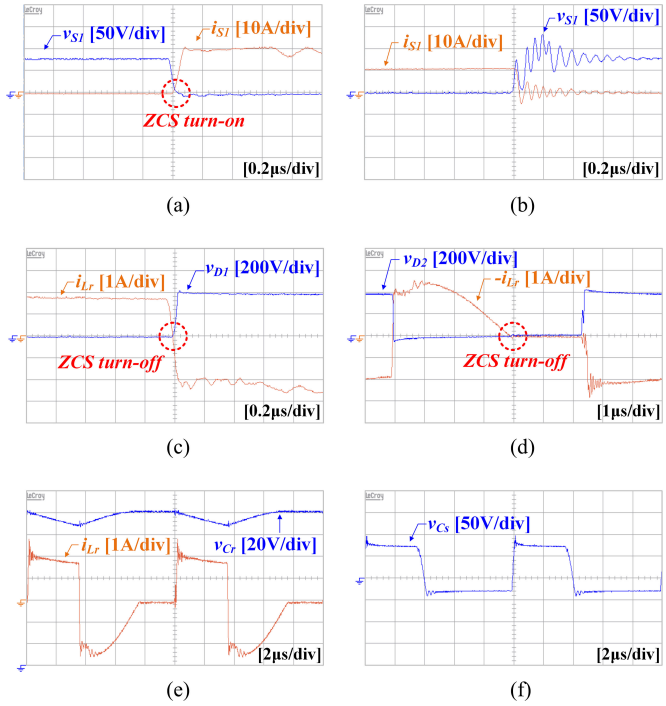

Fig. 10. Experimental waveforms at $V_i = 28$ V and $P_o = 250$ W: (a) switch S_1 at turn-on, (b) switch S_1 at turn-off, (c) diode D_1 at turn-off, (d) diode D_2 at turn-off, (e) current i_{Lr} and voltage v_{Cr}, and (f) voltage v_{Cs}.

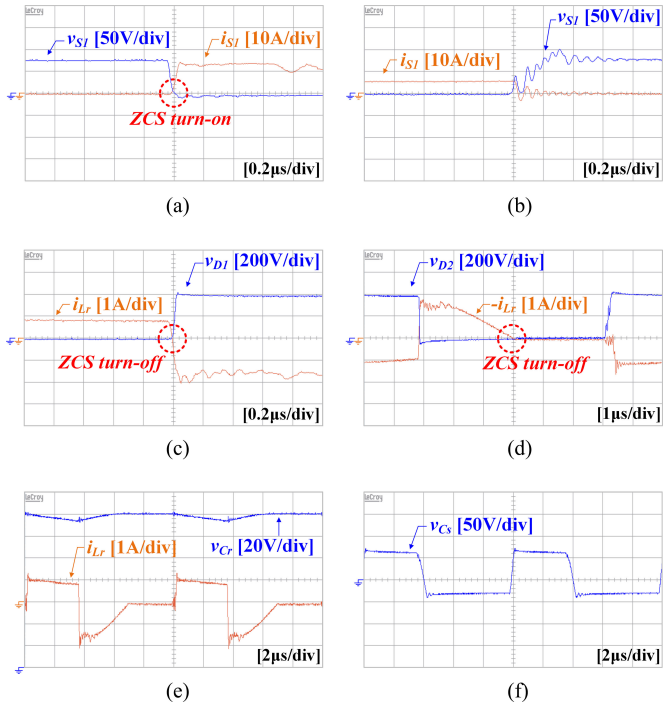

Fig. 11. Experimental waveforms at $V_i = 28$ V and $P_o = 125$ W: (a) switch S_1 at turn-on, (b) switch S_1 at turn-off, (c) diode D_1 at turn-off, (d) diode D_2 at turn-off, (e) current i_{Lr} and voltage v_{Cr}, and (f) voltage v_{Cs}.

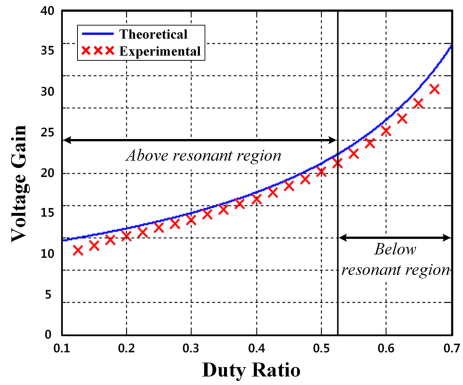

Fig. 12. Theoretical and experimental voltage gain of the proposed converter under $V_i = 28$ V, $R_o = 577\ \Omega$.

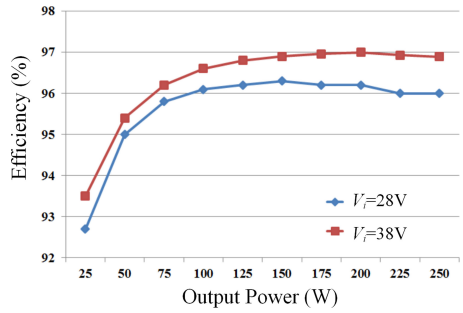

Fig. 13. Measured efficiency of the proposed converter.

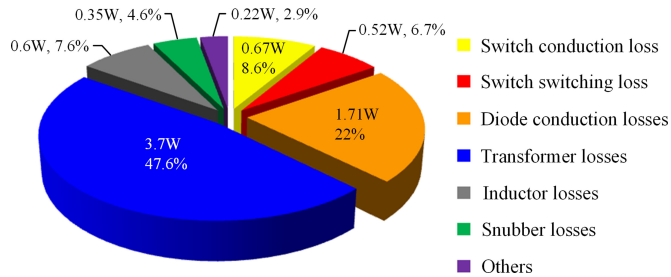

Fig. 14. Loss analysis of the proposed converter at full load ($V_i = 38$ V).

The efficiency of the proposed converter is measured by YOKOGAWA WT3000 and shown in Fig. 13. The maximum measured efficiency of the proposed converter is 97.0% at 200 W when input voltage is 38 V. The measured full-load efficiencies according to input voltage variation are 96.0% at $V_i = 28$ V and 96.9% at $V_i = 38$ V, respectively. The European efficiency of the proposed converter is 96.26%.

Fig. 14 shows loss analysis of the proposed converter at full load when input voltage is 38 V. The total loss of the proposed converter is 7.77 W. The large portion of the losses comes from losses of the transformer and conduction losses of diode D_1 and D_2, which are 47.6% and 22.0% of the total loss, respectively. Fig. 15 shows the photograph of the proposed prototype.

IV. Conclusion

In this paper, a soft-switched single switch isolated converter was proposed for step-up application such as MIC, portable fuel cell systems, and vehicle inverters. Improved features such

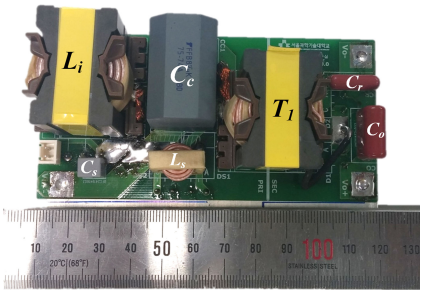

Fig. 15. Photograph of the proposed converter prototype.

as fully soft-switched characteristics of switch and diode, low-rated lossless snubber, and reduced transformer volume make the proposed converter achieve lower cost and higher power density compared to the conventional flyback-based converter. Experimental results on a 100 kHz, 250 W prototype are provided to validate the proposed concept. The maximum measured efficiency of 97.0% was obtained at 200 W.

REFERENCES

[1] Q. Li and P. Wolfs, "A review of the single phase photovoltaic module integrated converter topologies with three different dc link configurations," *IEEE Trans. Power Electron.*, vol. 23, no. 3, pp. 1320–1333, May 2008.

[2] N. D. Benavides and P. L. Chapman, "Mass-optimal design methodology for DC-DC converters in low-power portable fuel cell applications," *IEEE Trans. Power Electron.*, vol. 23, no. 3, pp. 1545–1555, May 2008.

[3] S. Y. Choe, J. W. Ahn, J. G. Lee, and S. H. Baek, "Dynamic simulator for a PEM fuel cell system with a PWM DC/DC converter," *IEEE Trans. Energy Convers.*, vol. 23, no. 2, pp. 669–680, Jun. 2008.

[4] H. Ma, L. Chen, and Z. Bai, "An active-clamping current-fed push-pull converter for vehicle inverter application and resonance analysis," in *Proc. IEEE Int. Symp. Ind. Electron.*, 2012, pp. 160–165.

[5] D. A. Ruiz-Caballero and I. Barbi, "A new flyback-current-fed push-pull DC-DC converter," *IEEE Trans. Power Electron.*, vol. 14, no. 6, pp. 1056–1064, Nov. 1999.

[6] M. Nymand and M. A. E. Andersen, "High-efficiency isolated boost DC-DC converter for high-power low-voltage fuel-cell applications," *IEEE Trans. Ind. Electron.*, vol. 57, no. 2, pp. 505–514, Feb. 2010.

[7] K. B. Park, G. W. Moon, and M. J. Youn, "Two-transformer current-fed converter with a simple auxiliary circuit for a wide duty range," *IEEE Trans. Power Electron.*, vol. 26, no. 7, pp. 1901–1912, Jul. 2011.

[8] F. J. Nome and I. Barbi, "A ZVS clamping mode-current-fed push–pull DC–DC converter," in *Proc. IEEE Int. Symp. Ind. Electron.*, vol. 2, 1998, pp. 617–621.

[9] V. Yakushev, V. Meleshin, and S. Fraidlin, "Full-bridge isolated current fed converter with active clamp," in *Proc. IEEE Appl. Power Electron. Conf. Expo.*, vol. 1, 1999, pp. 560–566.

[10] R. Watson and F. C. Lee, "A soft-switched, full-bridge boost converter employing an active clamp circuit," in *Proc. IEEE Conf. Power Electron. Spec. Conf. Rec.*, vol. 2, 1996, pp. 1948–1954.

[11] S. Han, H. Yoon, G. Moon, M. Youn, Y. Kim, and K. Lee, "A new active clamping zero-voltage switching PWM current-fed half-bridge converter," *IEEE Trans. Power Electron.*, vol. 20, no. 6, pp. 1271–1279, Nov. 2005.

[12] J. Kwon and B. Kwon, "High step-up active-clamp converter with input-current doubler and output-voltage doubler for fuel cell power systems," *IEEE Trans. Power Electron.*, vol. 1, no. 1, pp. 108–115, Jan. 2009.

[13] H. Kim, C. Yoon, and S. Choi, "An improved current-fed ZVS isolated boost converter for fuel cell application," *IEEE Trans. Power Electron.*, vol. 25, no. 9, pp. 2357–2364, Sep. 2010.

[14] C. D. Davidson, "Zero voltage switching isolated boost converter topology," in *Proc. IEEE 33rd Int. Telecommun. Energy Conf.*, Oct. 2011, pp. 1–8.

[15] G. Spiazzi, P. Mattavelli, and A. Costabeber, "High step-up ratio flyback converter with active clamp and voltage multiplier," *IEEE Trans. Power Electron.*, vol. 26, no. 11, pp. 3205–3214, Nov. 2011.

[16] B. York, W. Yu, and J.-S. Lai, "Hybrid-frequency modulation for PWM-integrated resonant converters," *IEEE Trans. Power Electron.*, vol. 28, no. 2, pp. 985–994, Feb. 2013.

[17] B. York, W. Yu, and J.-S. Lai, "An integrated boost resonant converter for photovoltaic applications," *IEEE Trans. Power Electron.*, vol. 28, no. 3, pp. 1199–1207, Mar. 2013.

[18] F. Evran and M. T. Aydemir, "Z-source-based isolated high step-up converter," *IET Power Electron.*, vol. 6, no. 1, pp. 117–224, Jan. 2013.

[19] F. Evran and M. T. Aydemir, "Isolated high step-up DC-DC converter with low voltage stress," *IEEE Trans. Power Electron.*, vol. 29, no. 7, pp. 3591–3603, Jul. 2014.

[20] K. B. Park, C. E. Kim, G. W. Moon, and M.-J. Youn, "PWM resonant single-switch isolated converter," *IEEE Trans. Power Electron.*, vol. 24, no. 8, pp. 1876–1886, Aug. 2009.

[21] W.-Y. Choi and J.-Y. Choi, "High-efficiency power conditioning system for grid-connected photovoltaic modules," *J. Power Electron.*, vol. 11, no. 4, pp. 561–567, Jul. 2011.

[22] C.-W. Roh, C.-H. Yoo, D.-Y. Jung, and S.-C. Sakong, "Polarity inversion DC–DC power conversion circuit with high voltage step-up ratio," *J. Power Electron.*, vol. 11, no. 5, pp. 669–676, Sep. 2011.

[23] J. H. Lee, T. J. Liang, and J. F. Chen, "Isolated coupled-inductor-integrated DC-DC converter with nondissipative snubber for solar energy applications," *IEEE Trans. Ind. Electron.*, vol. 61, no. 7, pp. 3337–3348, Jul. 2014.

[24] J.-M. Kwon, W.-Y. Choi, and B.-H. Kwon, "Single-switch quasi-resonant converter," *IEEE Trans. Ind. Electron.*, vol. 56, no. 4, pp. 1158–1163, Apr. 2009.

[25] J.-H. Lee, J.-H. Park, and J. H. Jeon, "Series-connected forward-flyback converter for high step-up power conversion," *IEEE Trans. Power Electron.*, vol. 26, no. 12, pp. 3629–3641, Dec. 2011.

[26] A. Emrani, E. Adib, and H. Farzanehfard, "Single-switch soft-switched isolated DC-DC converter," *IEEE Trans. Power Electron.*, vol. 27, no. 4, pp. 1952–1957, Apr. 2012.

[27] M. Matsuo, T. Suetsugu, S. Mori, and I. Sasase, "Class DE current-source parallel resonant inverter," *IEEE Trans. Ind. Electron.*, vol. 46, no. 2, pp. 242–248, Apr. 1999.

[28] Y. Ren, M. Xu, J. Zhou, and F. C. Lee, "Analytical loss model of power MOSFET," *IEEE Trans. Power Electron.*, vol. 21, no. 2, pp. 310–319, Mar. 2006.

[29] T. J. Liang, R. Y. Chen, and J. F. Chen, "Current-fed parallel-resonant dc–ac inverter for cold-cathode fluorescent lamps with zero-current switching," *IEEE Trans. Power Electron.*, vol. 23, no. 4, pp. 2206–2210, Jul. 2008.

Minjae Kim received the B.S. and M.S. degrees from the Seoul National University of Science and Technology, Seoul, Korea, in 2011 and 2013, respectively, where he is currently working toward the Ph.D. degree in the Power Electronics & Fuel Cell Power Conditioning Laboratory.

His research interests include dc–dc converter and battery charger for electric vehicles and renewable energy systems.

Sewan Choi (S'92–M'96–SM'04) received the B.S. degree in electronic engineering from Inha University, Incheon, Korea, in 1985, and the M.S. and Ph.D. degrees in electrical engineering from Texas A&M University, College Station, TX, USA, in 1992 and 1995, respectively.

From 1985 to 1990, he was with Daewoo Heavy Industries as a Research Engineer. From 1996 to 1997, he was a Principal Research Engineer at Samsung Electro-Mechanics Co., Korea. In 1997, he joined the Department of Electrical and Information Engineering, Seoul National University of Science and Technology, Seoul, Korea, where he is currently a Professor. His research interests include power conversion technologies for renewable energy systems and dc–dc converters and battery chargers for electric vehicles.

He is an Associate Editor of the IEEE TRANSACTIONS ON POWER ELECTRONICS and IEEE TRANSACTIONS ON INDUSTRY APPLICATIONS.